PERGAMON Computers and Mathematics with Applications 39 (2000) 131–149

An International Journal
computers & mathematics
with applications

www.elsevier.nl/locate/camwa

Image Denoising and Segmentation via Nonlinear Diffusion

YUNMEI CHEN
Department of Mathematics, University of Florida
Gainesville, FL 32611, U.S.A.
yun@math.ufl.edu

B. C. VEMURI* AND LI WANG
Department of Computer and Information Science and Engineering
University of Florida, Gainesville, FL 32611, U.S.A.
vemuri@cise.ufl.edu

(Received October 1998; revised and accepted May 1999)

Abstract—Image denoising and segmentation are fundamental problems in the field of image processing and computer vision with numerous applications. In this paper, we present a nonlinear PDE-based model for image denoising and segmentation which unifies the popular model of Alvarez, Lions and Morel (ALM) for image denoising and the Caselles, Kimmel and Sapiro model of geodesic "snakes". Our model includes nonlinear diffusive as well as reactive terms and leads to quality denoising and segmentation results as depicted in the experiments presented here. We present a proof for the existence, uniqueness, and stability of the viscosity solution of this PDE-based model. The proof is in spirit similar to the proof of the ALM model; however, there are several differences which arise due to the presence of the reactive terms that require careful treatment/consideration. A fast implementation of our model is realized by embedding the model in a scale space and then achieving the solution via a dynamic system governed by a coupled system of first-order differential equations. The dynamic system finds the solution at a coarse scale and tracks it continuously to a desired fine scale. We demonstrate the smoothing and segmentation results on several real images.

Keywords—Nonlinear diffusion, Image processing, Segmentation, PDEs, Scale-space tracking.

1. INTRODUCTION

Image denoising and segmentation are fundamental problems in the field of image processing and computer vision. Image denoising (or noise removal) is a technique that enhances images by reducing any degradations that may be present. The most common degradation source is the noise from the image acquisition system and is commonly modeled by Gaussian random noise in most cases. Another source of degradation is the so-called salt-and-pepper noise that can occur due to a random bit error in a communication channel during transmission. In the context of

Chen was supported in part by the NSF Grant DMS-9703497. Vemuri and Wang were supported in part by the NIH Grants RO1-LM05944 and RO1-RR13197 and the NSF Grant IIS-9811042. The authors would like to thank P. Mergo for providing the CT images and J. N. Wilson for providing the infrared images.
*Author to whom all correspondence should be addressed.

0898-1221/00/$ - see front matter Typeset by $\mathcal{A}\mathcal{M}\mathcal{S}$-TEX
PII: S0898-1221(00)00050-X

image segmentation, the most important step is detection of region boundaries or edges. An *edge* in an image may be defined as a location in the image at which a significant change occurs in image intensity. Segmented images contain very useful information and are used very often to convey the essential content of an image. Such image representations are useful in object recognition, low bit-rate image coding systems, and various other applications [1].

The problem of image denoising and segmentation can be posed in either a deterministic or a stochastic framework. Stochastic methods are quite effective in achieving segmentation but are limited by their intense computational requirements [2,3]. We will therefore limit ourselves to the deterministic formulations, specifically, partial differential equation (PDE) based methods that lend themselves to fast numerical implementations.

Image denoising and segmentation can be formulated using variational principles which in turn require solutions to PDEs. Recently, there has been a flurry of activity on the PDE-based segmentation schemes. In [4], Perona and Malik developed an *anisotropic diffusion* scheme for image smoothing and segmentation. The basic idea of this nonlinear smoothing scheme was to smooth the image while preserving the edges in it. This was done by using the equation $I_t = \mathrm{div}(c(\nabla I)\nabla I)$, where I is the image to be smoothed and I_t describes its evolution over time, and $c(\nabla I)$ is a decreasing function of ∇I. Segmentation was achieved by finding edges in this smoothed image. Catte *et al.* [5], Nitzberg and Mumford [6], and Alvarez *et al.* [7] recognized the ill-posedness of the Perona-Malik diffusion and proposed modifications to overcome the same. Since then, several nonlinear diffusion methods have been developed and a good account of these can be found in [8–10]. In [11], Kimia *et al.* proposed an interesting reaction-diffusion based theory which describes the shapes of objects in an entropy scale-space. This theory was later used by Tek and Kimia [12] for image segmentation applications.

Image segmentation can also be achieved by approaches based on *curve evolution*. Malladi *et al.* [13,14] and Caselles *et al.* [15] used curve evolution for recovering shapes from 2-D and 3-D images. The curve evolution equation was implemented by embedding the initial curve as a level curve in a surface and allowing all the level curves of the surface to evolve simultaneously. This level-set method has the advantage of being able to elegantly represent topological changes during the evolution of the curve and thereby allows recovery of shapes without *a priori* knowledge of their topology. The evolution equation used in [13–15] was $\frac{\partial \phi}{\partial t} = g(\nabla I)\|\nabla \phi\|(c + \kappa)$, where ϕ is the embedding surface for the curve evolution, $g(\nabla I) = 1/(1 + \|\nabla(G_\sigma * I)\|^2)$ is a stopping term applied on the curve evolution, $\kappa = \mathrm{div}(\nabla\phi/\|\nabla\phi\|)$ is the curvature of the level curves of ϕ, and c is a constant speed evolution term. This method was generalized by Caselles *et al.* [16] and Kichenassamy *et al.* [17] who also established the link between the curve evolution based methods and the very popular elasticity-based *snakes* (active contour models) [18–20] used for segmentation in computer vision and image processing literature. Another interesting curve smoothing using nonlinear diffusion technique was presented in [21], wherein the goal was to preserve certain salient features such as corners, etc., while smoothing irrelevant detail. This scheme was designed to be applicable only for closed curves and was derived from curvature (as opposed to arc length) minimization of a parameterized curve. This scheme could be applied to extract shape of boundaries of interest from images. In [22], Malladi and Sethian propose a unified approach to noise removal and image segmentation using the concept of min-max curvature flow. Based on the image data, a min/max switch was designed to select $\min(\kappa, 0.0)$ or $\max(\kappa, 0.0)$ so that the curvature based curve evolution smoothes out small oscillations, but maintains the essential properties of the shape. Results of implementation were shown on a variety of images yielding quality noise removal and image segmentation. Anisotropic diffusion filters that use a tensorial diffusivity parameter were introduced in [10]. These filters can be tailored to enhance image structures (edges, parallel lines, curves, etc.) that occur in preferred directions. More recently, Kimmel *et al.* [23] presented a very general flow called the Beltrami flow as a general framework for image smoothing and show that most flow-based smoothing schemes may be viewed as special cases in their framework.

In [9], Shah developed a common framework for curve evolution, image denoising and segmentation, and anisotropic diffusion. In this work, a new segmentation functional was developed which leads to a coupled system of PDEs; one of them performed nonlinear smoothing of the input image and the other smoothed an "edge strength" function. Shah [9] demonstrated that all the existing curve evolution and anisotropic diffusion schemes reported in literature can be viewed as special cases of his method.

Each of the methods we discussed above is in a variational form that minimizes an energy functional which in some cases is nonconvex. This nonconvex minimization is hard and most computationally feasible methods lead to suboptimal solutions. In [24,25], a coarse-to-fine scale space tracking technique was proposed as a means to efficiently achieve a significant optimum for the nonconvex optimization. In this approach, the desired solution is found by first finding a solution at a significantly coarser scale and then tracking it down through finer scales (see Figure 1). It was demonstrated that this technique can find significant minima of practical interest that exist over a large range of scale [24,25]. In our implementation, to achieve better computational performance, we use a similar approach to [24]. An alternative scale-space implementation involves the use of a multigrid approach as in Acton's work presented in [26]. The work described by Acton is a multigrid implementation of a diffusion equation which is quite different from the one presented here. However, we feel that it is worth investigating the possibility of applying such a multigrid approach to our nonlinear smoothing model and will consider it in our future work. For now, it suffices to note that the key difference between the scale-space tracking approach adopted here and the multigrid scheme is that the former involves solving a differential equation, and hence, involves a continuous scale tracking while the latter is a discrete scale only approach.

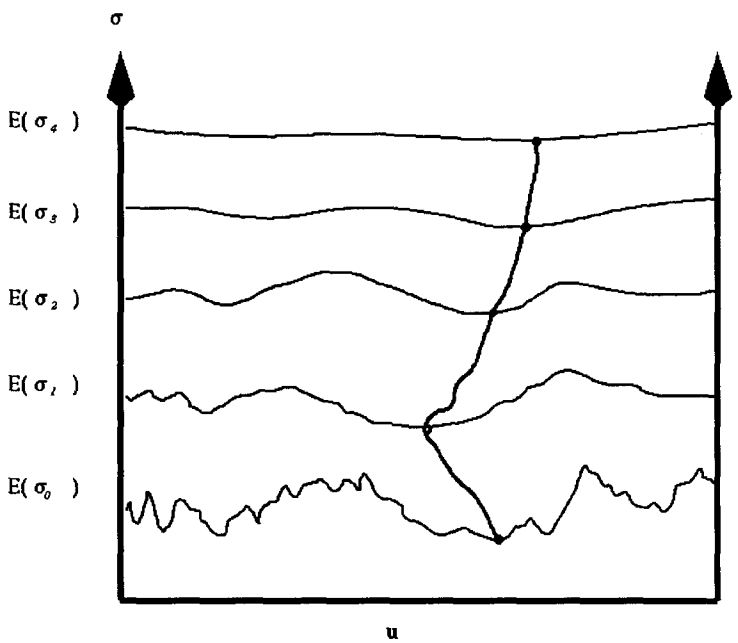

Figure 1. Scale space tracking: the desired solution is obtained by finding a solution at a coarser scale and then tracking it down through finer scales.

In this paper, we present a unified PDE-based image denoising and segmentation approach which is a combination/unification of the approaches due to Alvarez *et al.* [7] (ALM) and Caselles *et al.* [16,27] and is based on a nonlinear diffusion equation with additive reactive terms. The primary difference between our model and the ALM model is that our formulation involves a time varying diffusive coefficient, and our PDE has two additional terms that are not present in the ALM model. One of them is a reactive term used for image enhancement, and another is a term that ensures that the smoothed image is a close approximation of the original image.

In [28], Sapiro presents the idea of "self-snakes" as an interesting application of the "color-snakes" presented in the same and in [29]. There are some similarities between our work presented here and the idea of "self-snakes". The diffusivity coefficient in the "self-snakes" and our formulation look similar; however, the key difference is that in our formulation this coefficient is *time varying* which leads to a less noise-sensitive stopping criteria for the edge preserving nonlinear smoothing. Another difference between our formulation and the "self-snakes" is that there is no term to enforce the closeness of the smooth approximation to the original image in the "self-snakes".

We experimentally demonstrate that our unification model leads to superior smoothing—compared to the ALM model [7] and Shah's model [9]—on a synthetically generated highly noisy test image (signal to noise ratio being 1 : 2). We also prove the existence, uniqueness, and stability of the viscosity-solution for this "unified" model equation and present implementation details along with several experiments demonstrating the effectiveness of the proposed denoising and segmentation scheme.

The rest of the paper is organized as follows: in the next section, we present our new nonlinear diffusion model which is used for selective smoothing of images. In Section 3, we prove the existence, uniqueness, and stability of the viscosity solution of the model. Section 4 contains a description of the numerical methods used to implement the model equation. In Section 5, examples of results obtained using our new technique on a variety of image data are presented. We conclude the paper in Section 6.

2. NONLINEAR DIFFUSION MODEL

Numerous models of linear and nonlinear diffusion have been proposed in literature for achieving image smoothing and segmentation. A survey of various nonlinear methods is discussed in [10]. The linear models involved the standard heat equation $\partial_t u = \Delta u$ with $u(x,0) = f(x)$ where $f : \Re^2 \to \Re$ is a scalar valued image. This type of linear diffusion blurs important image features such as edges. In addition, it displaces the edges, i.e., when moving from finer to coarser scales, it dislocates the edges. In general, relating structures across scales is nontrivial due to the presence of bifurcations.

Nonlinear anisotropic diffusion has been proposed by many researchers [4,5,7,30]. All of these are nonlinear models and differ in the diffusivity coefficient and/or the diffusion term. Some of them are also supplemented with a reactive term. In the following, we present a nonlinear diffusion equation supplemented with reactive terms for achieving edge preserving smoothing and segmentation.

Our model takes the following form:

$$\frac{\partial u}{\partial t} = g(\nabla G_\sigma * u)|\nabla u| \operatorname{div}\left(\frac{\nabla u}{|\nabla u|}\right) + \nabla g(\nabla G_\sigma * u) \cdot \nabla u \tag{1}$$

$$-\beta|\nabla u|(u - I) \tag{2}$$

$$\left.\frac{\partial u}{\partial n}\right|_{\partial R} = 0, \qquad u_0 = I, \tag{3}$$

where $I(x,y)$ is the intensity image to be processed, $u(x,y,t)$ is its smoothed version, β is a weighting parameter, $G_\sigma(x,y) = (1/4\pi\sigma)\exp\{-(x^2+y^2)/(2\pi\sigma^2)\}$ is a Gaussian smoothing kernel with a prespecified σ, and $g(s) = 1/(1+\|s\|^2/K)$ is a nonincreasing real valued function (for $s > 0$) which tends to zero as $s \to \infty$ with a constant K.

Purely for the sake of interpretation, this equation may be posed as the minimization of the following energy functional for fixed v, where $v = \nabla G_\sigma * u$—this, however, is not what is done in our approach since $g(v)$ is not really a constant. Note that the variation is taken with respect to u for a fixed v:

$$E_v(u) = \int\int_R \left\{g(v)|\nabla u| + \beta(u - I)^2\right\} dx\, dy. \tag{4}$$

From this functional, it is easy to see the following.

1. The coefficient of the first term, namely, $g(\nabla G_\sigma * u)$ serves the purpose of selecting the locations in the image for smoothing. For instance, at image locations having large values of gradient, this coefficient takes on a small value, thereby reducing the smoothing performed at these locations since $g(s)$ is a nonincreasing function of s.
2. The term $|\nabla u|$ regularizes the solution u and is responsible for the nonlinear term $|\nabla u|$ $\operatorname{div}(\nabla u/|\nabla u|)$ in equation (2). It diffuses u in a direction away from that of ∇u.
3. The term $(u - I)^2$ forces u to be a close approximation to the data I.

Note that our model is different from the one reported in [7] in that it yields two additional terms in the Euler-Lagrange PDE in equation (2)—a.k.a. the gradient descent equation—for the variation principle in equation (4). These two reactive terms are responsible for forcing the evolution-based image smoothing to stop at the edges and the resulting solution to be close approximation to the original image data, respectively. Our model is also different from the one reported in [31] wherein the reactive term was used to accommodate the image quantization application. Our model is in spirit similar to the smoothing equation in [9]; however, the diffusivity coefficient is very different in our case.

For a *fast implementation* and to obtain quality smoothing and segmentation results, the scale parameter σ in the functional in equation (4) can be varied from large (coarse) to small (fine) values using a scale space tracking scheme. The scale space tracking can be posed as the steady state solution of a differential equation obtained by differentiating the equation representing the equilibrium condition of the functional in equation (4) with respect to σ. The resultant differential equation describing the scale space trajectory is, however, very complicated. A simpler coupled system of equations for tracking the solution across scale (from coarse-to-fine σ) for this nonlinear diffusion model can be obtained using the approach described in [24]. The coupled system of scale space equations are given by

$$\begin{aligned} \frac{\partial u}{\partial t} &= -\nabla E_v(u, \sigma), \\ \frac{\partial \sigma}{\partial t} &= -c_1 e^{-c_2 |\nabla E_v(u,\sigma)|}, \end{aligned} \tag{5}$$

where c_1 and c_2 are prespecified constants. For a set of initial u_0 and σ_0 which is far away from the solution, $\nabla E_v(u, \sigma)$ is large while $-c_1 e^{-c_2|\nabla E(u,\sigma)|}$ is small, thus equation (5) is solved for u at a nearly constant scale until a solution at this scale is found. Once a solution is obtained, it satisfies $\frac{\partial u}{\partial t} = 0$ and $\frac{\partial \sigma}{\partial t} = -c_1$. Equation (5) can then be used to track the solution down to finer scales. This technique is computationally efficient and yields quality smoothing and segmentation results as is demonstrated in our experiments. Note that the proof of existence, uniqueness, and stability of a viscosity solution of our model presented in the following section does not hold for the above-described coupled system of scale-space tracking equations.

3. EXISTENCE, UNIQUENESS, AND STABILITY

Since our model (3) is highly nonlinear and degenerate, we need the notion of so-called viscosity solution (see [32]). In this section, we will prove the existence, uniqueness, and stability for the viscosity solution to the equation (3).

The well-posedness of the viscosity solution of the mean curvature flow $u_t - |\nabla u| \operatorname{div}(\nabla u/|\nabla u|) = 0$, in $R^n \times R_+$ and for the generalized mean curvature flow $u_t - |\nabla u|(\operatorname{div}(\nabla u/|\nabla u|) + \gamma) = 0$, in $R^n \times R_+$, $\gamma \in R$, were studied by Evans and Spruck [33] and by Chen, Giga and Goto [34], respectively. In [7], the existence, uniqueness, and stability for the viscosity solution of the following highly nonlinear diffusion equation: $u_t - g(\nabla G_\sigma * u)|\nabla u|(\operatorname{div}(\nabla u/|\nabla u|) = 0$, in $R^n \times R_+$, where $g(p) = 1/(1 + |p|^2)$ was established. Viscosity analysis for the level set form of the active contour model $u_t - g(\nabla G_\sigma * I)|\nabla u|(\operatorname{div}(\nabla u/|\nabla u|) + \gamma) + \nabla g \cdot \nabla u = 0$, in $R^2 \times R_+$, $\gamma \in R$, where $I(x, y)$ is the initial surface embedding the initial contour, was briefly discussed in [16,17].

Our model has a similar structure, but more nonlinear terms than in the models mentioned above. The proof of well-posedness for our model follows the ideas in [7]. However, since our model has more nonlinear factors or terms than the models mentioned above, more careful and delicate estimates are required, especially in getting the uniform L^∞-norm estimate for the gradient of the approximate solutions and in establishing the estimate $\sup_{\Omega\times[0,T]}|u-v| \le C\sup_{\Omega\times\{t=0\}}|u-v|$, where u and v are two viscosity solutions of (3).

Our model equation (2) is in two dimensions, but mathematically we can study this problem for n-dimensional cases. σ, β, and K are constants in (2), and they do not effect the proof of well-posedness. To simplify the presentation, we shall consider $\sigma = \beta = K = 1$ and work with periodic boundary conditions similar to the presentation in [7]. Then, by periodic extension we consider the following Cauchy problem:

$$\begin{aligned} \frac{\partial u}{\partial t} &= g(\nabla G * u)a_{ij}(\nabla u)u_{x_ix_j} \\ &\quad + \frac{\partial g}{\partial l}(\nabla G * u)[(\nabla G_{x_l} * u)\cdot\nabla u] - |\nabla u|(u-I), \qquad x\in R^n, \quad t\in R_+, \\ u(x,0) &= I(x), \qquad x\in R^n, \end{aligned} \tag{6}$$

where $G = (1/4\pi)\exp\{-(x^2+y^2)/4\}$, $g(p) = 1/(1+|p|^2)$, $a_{ij}(p) = \delta_{ij} - p_ip_j/|p|^2$, and the summation convention is used.

First, let us recall the definition of viscosity subsolution of (6). A function $u\in C([0,T]\times R^n)$ for some $T>0$ is said to be a viscosity subsolution of (6), if for all $\phi\in C^2(R^2\times R)$, the following condition holds at any point $(x_0,t_0)\in R^n\times(0,T]$, at which $(u-\phi)$ attains a local maximum:

$$\begin{aligned} &\frac{\partial\phi}{\partial t}(x_0,t_0) - g((\nabla G*u)(x_0,t_0))a_{ij}(\nabla\phi(x_0,t_0))\phi_{x_ix_j}(x_0,t_0) \\ &\quad + \frac{\partial g}{\partial l}((\nabla G*u)(x_0,t_0))[(\nabla G_{x_l}*u)(x_0,t_0)\cdot\nabla\phi(x_0,t_0)] \\ &\quad - |\nabla\phi(x_0,t_0)|(u-I)(x_0,t_0) \le 0, \qquad \text{if } \nabla\phi(x_0,t_0)\neq 0, \end{aligned} \tag{7}$$

$$\begin{aligned} &\frac{\partial\phi}{\partial t}(x_0,t_0) - g((\nabla G*u)(x_0,t_0))\limsup_{p\to 0} a_{ij}(p)\phi_{x_ix_j}(x_0,t_0) \le 0, \\ &\qquad\qquad \text{if } \nabla\phi(x_0,t_0) = 0. \end{aligned} \tag{8}$$

A viscosity supersolution is similarly defined by substituting "local maximum" for "local minimum", "≤ 0" for "≥ 0", and "limsup" for "liminf" in equations (7) and (8), respectively. A viscosity solution is a continuous function which is both a subsolution and a supersolution. We now state and prove the main theorem of this paper.

THEOREM 3.1. *The Cauchy problem (6) has a unique viscosity solution $u\in C(R^n\times[0,T])\cap L^\infty(0,T;W^{1,\infty}(R^n))$ for any $T\in[0,\infty)$, and $\inf_{R^n} I \le u(x,t) \le \sup_{R^n} I$, provided that I is Lipschitz continuous on R^n.*

Moreover, if $v\in C(R^n\times R_+)$ is a viscosity solution of (6) with I replaced by a Lipschitz continuous function I_1, then for all $T\in[0,+\infty)$, there exists a constant $C>0$, depending only on I, I_1, and T, such that

$$\sup_{0\le t\le T}\|u(x,t)-v(x,t)\|_{L^\infty(R^n)} \le C\|I-I_1\|_{L^\infty(R^n)}.$$

PROOF. In the following, we present the proof in three stages.

STEP 1. We first show that if u is a viscosity solution of (6) on $R^n\times R_+$, then

$$\inf_{R^n} I \le u \le \sup_{R^n} I, \qquad \text{on } R^n\times[0,\infty). \tag{9}$$

Let $\phi = \sup_{R^n} I + \delta t$ (where $\delta > 0$) in (7) and assume that $u - \phi$ attains a local maximum at (x_0, t_0) with $t_0 > 0$, then $\nabla\phi(x_0, t_0) = 0$ and from equation (7), $\frac{\partial\phi}{\partial t}(x_0, t_0) \le 0$. This contradicts $\frac{\partial\phi}{\partial t} \equiv \delta > 0$ on $R^n \times [0, \infty)$. Therefore, $u - \phi$ must attain its maximum at $t_0 = 0$. So,

$$u - \phi \le \sup\left(I - \sup_{R^n} I\right),$$

$$u \le \sup_{R^n} I + \delta t.$$

Similarly, we have (from the definition of supersolution)

$$u \ge \inf_{R^n} I - \delta t.$$

Letting $\delta \to 0$ proves (9).

STEP 2. Next we prove the gradient estimate for the approximate solution. Consider the following Cauchy problem:

$$\begin{aligned} \frac{\partial u^\varepsilon}{\partial t} &= g^\varepsilon(\nabla G * u^\varepsilon) a_{ij}^\varepsilon(\nabla u^\varepsilon) u^\varepsilon_{x_i x_j} \\ &\quad + \frac{\partial g^\varepsilon}{\partial l}(\nabla G * u^\varepsilon)[(\nabla G_{x_l} * u^\varepsilon) \cdot \nabla u^\varepsilon], \qquad x \in R^n, \quad t \in R_+, \\ &\quad - b^\varepsilon(\nabla u^\varepsilon)(u^\varepsilon - I^\varepsilon), \\ u^\varepsilon(x, 0) &= I^\varepsilon(x), \qquad x \in R^n, \end{aligned} \tag{10}$$

where

$$\begin{aligned} &0 < \varepsilon < 1, \\ &g^\varepsilon(s) = g(s) + \varepsilon, \\ &a_{ij}^\varepsilon(p) = (\varepsilon + 1)\delta_{ij} - \frac{P_i P_j}{|P|^2 + \varepsilon^2}, \\ &b^\varepsilon(p) = \sqrt{|p|^2 + \varepsilon}, \\ &I^\varepsilon \in C^\infty(R^n) \text{ (periodic) such that } I^\varepsilon \to I \text{ uniformly, and} \\ &\|\nabla I^\varepsilon\|_{L^\infty(R^n)} \le \|\nabla I\|_{L^\infty(R^n)}, \qquad \|I^\varepsilon\|_{L^\infty(R^n)} \le \|I\|_{L^\infty(R^n)}. \end{aligned}$$

By the theory of quasi-linear uniformly parabolic equations [35, Section 6, Theorem 4.4], the problem (10) admits a smooth solution $u^\varepsilon \in C^\infty(R^n \times R_+)$. Since any smooth solution is a viscosity solution, by an argument similar to that in Step 1, we know that

$$|u^\varepsilon| \le M, \qquad \text{for } (x, t) \in R^n \times [0, \infty), \tag{11}$$

where $M > 0$ is a constant depending only on I. Now we shall show a uniform estimate for $|\nabla u^\varepsilon|_{L^\infty(R^n)}$.

Differentiating (10) with respect to x_k, then multiplying the resulting equation by $2u^\varepsilon_{x_k}$ and taking a summation w.r.t. k, we get

$$\begin{aligned} &\frac{\partial|\nabla u^\varepsilon|^2}{\partial t} - g^\varepsilon(\nabla G * u^\varepsilon) a_{ij}^\varepsilon(\nabla u^\varepsilon) \frac{\partial^2|\nabla u^\varepsilon|^2}{\partial x_i \partial x_j} - g^\varepsilon(\nabla G * u^\varepsilon) \frac{\partial a_{ij}^\varepsilon}{\partial l}(\nabla u^\varepsilon) u^\varepsilon_{x_i x_j} \frac{\partial|\nabla u^\varepsilon|^2}{\partial x_l} \\ &\quad - \frac{\partial g^\varepsilon}{\partial l}(\nabla G * u^\varepsilon)(\nabla G_{x_l} * u^\varepsilon) \cdot (\nabla|\nabla u^\varepsilon|^2) + \frac{\partial b^\varepsilon(\nabla u^\varepsilon)}{\partial m}(u^\varepsilon - I^\varepsilon) \frac{\partial|\nabla u^\varepsilon|^2}{\partial x_m} \\ &\qquad = 2\frac{\partial g^\varepsilon}{\partial l}(\nabla G * u^\varepsilon)(G_{x_l x_k} * u^\varepsilon) a_{ij}^\varepsilon(\nabla u^\varepsilon) u^\varepsilon_{x_i x_j} u^\varepsilon_{x_k} \\ &\qquad + 2\frac{\partial^2 g^\varepsilon}{\partial l \partial m}(\nabla G * u^\varepsilon)(G_{x_m x_k} * u^\varepsilon)(\nabla G_{x_l} * u^\varepsilon \cdot \nabla u^\varepsilon) u^\varepsilon_{x_k} \\ &\qquad + 2\frac{\partial g^\varepsilon}{\partial l}(\nabla G * u^\varepsilon)[(\nabla G_{x_l x_k} * u^\varepsilon) \cdot \nabla u^\varepsilon] u^\varepsilon_{x_k} \\ &\quad - 2g^\varepsilon(\nabla G * u^\varepsilon) a_{ij}^\varepsilon(\nabla u^\varepsilon) u^\varepsilon_{x_k x_i} u^\varepsilon_{x_k x_j} - 2b^\varepsilon(\nabla u^\varepsilon)(u^\varepsilon_{x_k} - I^\varepsilon_{x_k}) u^\varepsilon_{x_k}. \end{aligned} \tag{12}$$

From the definitions of a_{ij}^{ε}, b^{ε}, g^{ε}, and G, we have

$$\left|a_{ij}^{\varepsilon}(\nabla u^{\varepsilon})u_{x_ix_j}^{\varepsilon}\right|^2 \le 2a_{ij}^{\varepsilon}(\nabla u^{\varepsilon})u_{x_kx_i}^{\varepsilon}u_{x_kx_j}^{\varepsilon},$$
$$\left|\frac{\partial g}{\partial l}(\nabla G * u^{\varepsilon})\right|^2 \le 2g^{\varepsilon}(\nabla G * u^{\varepsilon}),$$

and for any multi-index α with $|\alpha| \le 2$,

$$\sup_{R^n\times R_+}|\nabla^{\alpha}G * u^{\varepsilon}| \le C, \qquad \sup_{R^n}\left|D_p^{\alpha}g^{\varepsilon}(p)\right| \le C, \qquad \sup_{R^n}|D_s^{\alpha}b^{\varepsilon}(s)| \le C, \tag{13}$$

where $C > 0$ is a constant depending only on M in (11).

Inserting these estimates into (12) and using Cauchy's inequality, we have

$$\text{RHS of (12)} \le C\left(|\nabla u^{\varepsilon}|^2 + 1\right), \qquad \text{in } R^n \times R_+, \tag{14}$$

where $C > 0$ is a constant depending only on M in (11), hence, C depends only on I. Applying the maximum principle [36] to (14) yields for all $t \in [0,T]$ (for any $T < \infty$),

$$\begin{aligned}\|\nabla u^{\varepsilon}(\cdot,t)\|_{L^{\infty}(R^n)} &\le e^{ct}\|\nabla I^{\varepsilon}\|_{L^{\infty}(R^n)}\\ &\le e^{ct}\|\nabla I\|_{L^{\infty}(R^n)} \le C_T,\end{aligned} \tag{15}$$

where $C_T > 0$ depends only on T and I. This implies that

$$|u^{\varepsilon}(x,t) - u^{\varepsilon}(y,t)| \le C_T|x-y|, \qquad \forall x, y \in R^n \quad \text{and} \quad \forall t \in [0,T].$$

By the same argument used in [32], we have

$$|u^{\varepsilon}(x,s) - u^{\varepsilon}(x,t)| \le C_T|t-s|^{1/2}, \qquad \forall x \in R^n \quad \text{and} \quad \forall s,t \in [0,T].$$

Then, by the Ascoli-Arzela theorem, there exists a subsequence u^{ε_k} of u^{ε}, and a function $u \in C(R^n \times [0,T]) \cap L^{\infty}(0,T;W^{1,\infty}(R^n))$ such that as $\varepsilon_k \to 0$,

$$u^{\varepsilon_k} \to u, \qquad \text{locally uniformly in } R^n \times R_+. \tag{16}$$

STEP 3. EXISTENCE OF VISCOSITY SOLUTION (16). We assert now that u obtained in (16) is a viscosity solution of (6) in the sense of (7) and (8).

Let $\phi \in C^2(R^n \times R)$ and assume $u - \phi$ has a strict local maximum at a point $(x_0,t_0) \in R^n \times R_+$. As $u^{\varepsilon_k} \to u$ uniformly near (x_0,t_0), $u^{\varepsilon_k} - \phi$ has a local maximum at a point (x_k,t_k) with

$$(x_k,t_k) \to (x_0,t_0), \qquad \text{as } k \to \infty \tag{17}$$

and at (x_k,t_k)

$$\nabla u^{\varepsilon_k} = \nabla\phi, \quad u_t^{\varepsilon_k} = \phi_t, \qquad a_{ij}^{\varepsilon_k}(\nabla u^{\varepsilon_k})u_{x_ix_j}^{\varepsilon_k} \le a_{ij}^{\varepsilon_k}(\nabla\phi)\phi_{x_ix_j}. \tag{18}$$

Therefore, (10) implies that at (x_k,t_k),

$$\begin{aligned}\frac{\partial\phi}{\partial t} - g^{\varepsilon_k}(\nabla G * u^{\varepsilon_k})a_{ij}^{\varepsilon_k}(\nabla\phi)\phi_{x_ix_j} - \frac{\partial g^{\varepsilon_k}}{\partial l}(\nabla G * u^{\varepsilon_k})[\nabla G_{x_l} * u^{\varepsilon_k}\cdot\nabla\phi]\\ + b^{\varepsilon_k}(\nabla\phi)(u^{\varepsilon_k} - I^{\varepsilon_k}) \le 0.\end{aligned} \tag{19}$$

If $\nabla\phi(x_0,t_0) \neq 0$, from (17), for sufficiently large k, $\nabla\phi(x_k,t_k) \neq 0$. One may apply limits in (19) to obtain (recalling the definitions of a_{ij}^{ε}, g^{ε}, b^{ε}, and (16),(17))

$$\begin{aligned}\frac{\partial\phi}{\partial t} - g(\nabla G * u)a_{ij}(\nabla\phi)\phi_{x_ix_j} - \frac{\partial g}{\partial l}(\nabla G * u)[(\nabla G_{x_l} * u)\cdot\nabla\phi] \\ + b(\nabla\phi)(u-I) \leq 0, \qquad \text{at } (x_0,t_0),\end{aligned} \tag{20}$$

which is the same as (7).

If $\nabla\phi(x_0,t_0) = 0$, let

$$h^k = \frac{\nabla\phi(x_k,t_k)}{\sqrt{|\nabla\phi(x_k,t_k)|^2+\varepsilon^2}},$$

then (19) reduces to

$$\begin{aligned}&\frac{\partial\phi}{\partial t} - g^{\varepsilon_k}(\nabla G * u^{\varepsilon_k})\left((\varepsilon_k+1)\delta_{ij} - h_i^k h_j^k\right)\phi_{x_ix_j} \\ &\quad - \frac{\partial g^{\varepsilon_k}}{\partial l}(\nabla G * u^{\varepsilon_k})[(\nabla G_{x_l} * u^{\varepsilon_k})\cdot\nabla\phi] \\ &\quad + b^{\varepsilon_k}(\nabla\phi)(u^{\varepsilon_k} - I^{\varepsilon_k}) \leq 0 \qquad \text{at } (x_k,t_k).\end{aligned} \tag{21}$$

Since $\nabla\phi(x_k,t_k) \to 0$, $\varepsilon_k \to 0$ as $k \to \infty$, hence, $b^{\varepsilon_k}(\nabla\phi(x_k,t_k)) \to 0$. Moreover, because $|h^k| \leq 1$, there is a subsequence of h^k, also denoted by h^k, such that as $k \to \infty$, $h^k \to h$ in $R^n \times R$ with $|h| \leq 1$. Applying limits to (21), we get

$$\frac{\partial\phi}{\partial t} - g(\nabla G * u)(\delta_{ij} - h_ih_j)\phi_{x_ix_j} \leq 0 \qquad \text{at } (x_0,t_0). \tag{22}$$

This is the same as (8). If $u-\phi$ has a local maximum, but not necessarily a strict local maximum at (x_0,t_0), we just need to repeat the argument above with $\phi(x,t)$ replaced by $\tilde{\phi}(x,t) = \phi(x,t) + |x-x_0|^4 + (t-t_0)^4$. Therefore, u is a subsolution of (6). Similarly, we can show that u is a supersolution. Hence, u is a viscosity solution of (6).

STEP 4. UNIQUENESS. Let u be a viscosity solution of (6) with Lipschitz continuous initial data I and v be a viscosity solution of (6) with I replaced by a Lipschitz continuous function I_1. Let

$$\omega(x,y,t) = u(x,t) - v(y,t) - (4\delta)^{-1}|x-y|^4 - \lambda t, \qquad t \in [0,T], \quad x,y \in R^n,$$

where $\delta > 0$ and $\lambda > 0$ are constants to be determined later.

CLAIM. $\omega(x,y,t)$ attains maximum at $t=0$ for an arbitrary positive constant λ.

Indeed, if $\omega(x,y,t)$ attains its maximum at some point (x_0,y_0,t_0) with $t_0 > 0$, by Theorem 8.3 in [32], for each $\mu > 0$, there exist X and Y, $(n\times n)$-symmetric matrices, and $\alpha,\beta \in R$, such that

$$\alpha - \beta = \lambda, \tag{23}$$

$$\begin{pmatrix} X & 0 \\ 0 & -Y \end{pmatrix} \leq A + \mu A^2, \tag{24}$$

and

$$\begin{aligned}&\alpha - g((\nabla G * u)(x_0,t_0))a_{ij}\left(\delta^{-1}|x_0-y_0|^2(x_0-y_0)\right)X_{ij} \\ &- \frac{\partial g}{\partial l}((\nabla G * u)(x_0,t_0))\left[(\nabla G_{x_l} * u)(x_0,t_0)\cdot\delta^{-1}|x_0-y_0|^2(x_0-y_0)\right] \\ &\quad + \delta^{-1}|x_0-y_0|^3(u(x_0,t_0) - I(x_0)) \leq 0,\end{aligned} \tag{25}$$

$$\begin{aligned}&\beta - g((\nabla G * v)(y_0,t_0))a_{ij}\left(\delta^{-1}|x_0-y_0|^2(x_0-y_0)\right)Y_{ij} \\ &- \frac{\partial g}{\partial l}((\nabla G * v)(y_0,t_0))\left[(\nabla G_{x_l} * v)(y_0,t_0)\cdot\delta^{-1}|x_0-y_0|^2(x_0-y_0)\right] \\ &\quad + \delta^{-1}|x_0-y_0|^3(v(y_0,t_0) - I_1(y_0)) \geq 0,\end{aligned} \tag{26}$$

where

$$A = (A_{ij})_{n\times n} \text{ and}$$
$$A_{ij} = \delta^{-1}|x_0 - y_0|^2\delta_{ij} + 2\delta^{-1}(x_0 - y_0)_i(x_0 - y_0)_j, \tag{27}$$

here $(x_0 - y_0)_i$ stands for the i^{th} component of $x_0 - y_0$.

We observe that $x_0 \neq y_0$. Indeed, if $x_0 = y_0$, then from (27), $A = 0$, hence, $X \leq 0$ and $Y \geq 0$ from (24). Thus, (25),(26) leads to $\alpha \leq 0$ and $\beta \geq 0$, which contradicts $\alpha - \beta = \lambda > 0$. We now choose

$$\mu = \delta|x_0 - y_0|^{-2}. \tag{28}$$

From (27) and (24) after some algebra, we have

$$\begin{pmatrix} X & 0 \\ 0 & -Y \end{pmatrix} \leq 2\delta^{-1}\begin{pmatrix} B & -B \\ -B & B \end{pmatrix}, \tag{29}$$

where

$$B_{ij} = |x_0 - y_0|^2\delta_{ij} + 5(x_0 - y_0)_i(x_0 - y_0)_j, \qquad 1 \leq i, j \leq n.$$

Let

$$U = (\nabla G * u)(x_0, t_0), \qquad V = (\nabla G * v)(y_0, t_0),$$
$$D = \left(a_{ij}\left(\delta^{-1}|x_0 - y_0|^2(x_0 - y_0)\right)\right)_{1\leq i.j\leq n},$$

and

$$Q = \begin{pmatrix} g(U)D & \sqrt{g(U)g(V)}D \\ \sqrt{g(U)g(V)}D & g(V)D \end{pmatrix}.$$

Noting that Q is a nonnegative symmetric matrix, from (29) we have

$$Q\begin{pmatrix} X & 0 \\ 0 & -Y \end{pmatrix} \leq 2\delta^{-1}Q\begin{pmatrix} B & -B \\ -B & B \end{pmatrix}.$$

Taking the trace, we get

$$g(U)D_{ij}X_{ij} - g(V)D_{ij}Y_{ij} \leq 4\delta^{-1}\left(\sqrt{g(U)} - \sqrt{g(V)}\right)^2|x_0 - y_0|^2. \tag{30}$$

Then, from (23) and (25),(26),

$$\lambda = \alpha - \beta \leq \mathrm{I} + \mathrm{II} + \mathrm{III}, \tag{31}$$

where

$$\mathrm{I} = g(U)D_{ij}X_{ij} - g(V)D_{ij}Y_{ij}, \tag{32}$$
$$\mathrm{II} = \left[\frac{\partial g}{\partial l}(U)(\nabla G_{x_l} * u)(x_0, t_0) - \frac{\partial g}{\partial l}(V)(\nabla G_{x_l} * v)(y_0, t_0)\right] \cdot \delta^{-1}|x_0 - y_0|^2(x_0 - y_0), \tag{33}$$
$$\mathrm{III} = \delta^{-1}|x_0 - y_0|^3[(u(x_0, t_0) - v(y_0, t_0)) + (I(x_0) - I_1(y_0))]. \tag{34}$$

We now estimate (32)–(34). First, for any multi-index α, $|\alpha| \leq 2$,

$$\begin{aligned}&(\nabla^\alpha G * u)(x_0, t_0) - (\nabla^\alpha G * v)(y_0, t_0)| \\ &\leq |(\nabla^\alpha G * u)(x_0, t_0) - (\nabla^\alpha G * v)(x_0, t_0)| + |(\nabla^\alpha G * v)(x_0, t_0) - (\nabla^\alpha G * v)(y_0, t_0)|,\end{aligned} \tag{35}$$

where constant $C > 0$ depends only on I and I_1 (as evident from (9)) and the Lipschitz constants for u and v. Then, by the mean value theorem, we have

$$\sqrt{g(U)} - \sqrt{g(V)} \leq C|U - V|, \tag{36}$$

$$\begin{aligned}&\left|\frac{\partial g}{\partial l}(U)(\nabla G_{x_l} * u)(x_0,t_0) - \frac{\partial g}{\partial l}(V)(\nabla G_{x_l} * v)(y_0,t_0)\right| \\ &\quad \le \left|\frac{\partial g}{\partial l}(U) - \frac{\partial g}{\partial l}(V)\right| |(\nabla G_{x_l} * u)(x_0,t_0)| \\ &\quad + \left|\frac{\partial g}{\partial l}(V)\right| |(\nabla G_{x_l} * u)(x_0,t_0) - (\nabla G_{x_l} * v)(y_0,t_0)|.\end{aligned} \tag{37}$$

It is easy to see

$$|u(x_0,t_0) - v(y_0,t_0)| + |I(x_0) - I_1(y_0)| \le C\left(\sup_{R^n\times[0,T]} |u-v| + |x_0 - y_0|\right). \tag{38}$$

The constants $C > 0$ in (35)–(38) depend only on I, I_1, and the Lipschitz constants for u and v.

Inserting (35)–(38) into (31)–(34) yields

$$\lambda \le C\delta^{-1}\left[\left(\sup_{R^n\times[0,T]} |u-v|\right)^2 |x_0-y_0|^2 + |x_0-y_0|^4 + \left(\sup_{R^n\times[0,T]} |u-v|\right)|x_0-y_0|^3\right]. \tag{39}$$

On the other hand, since (x_0, y_0, t_0) is the maximum point of $\omega(x,y,t)$,

$$u(x_0,t_0) - v(x_0,t_0) - (4\delta)^{-1}|x_0-y_0|^4 - \lambda t_0 \ge u(y_0,t_0) - v(y_0,t_0) - \lambda t_0.$$

This leads to

$$|x_0 - y_0| \le (4\delta L)^{1/3}, \tag{40}$$

where L is a Lipschitz constant for u in $R^n \times [0,T]$. Combining this with (39) yields

$$\begin{aligned}\lambda &\le C\delta^{-1}\left\{\left(\sup_{R^n\times[0,T]} |u-v|\right)^2 (4\delta L)^{2/3} + \left(\sup_{R^n\times[0,T]} |u-v|\right) 4\delta L + (4\delta L)^{4/3}\right\} \\ &\le C_0\left\{\delta^{-1/3}\left(\sup_{R^n\times[0,T]} |u-v|\right)^2 + \sup_{R^n\times[0,T]} |u-v| + \delta^{1/3}\right\},\end{aligned} \tag{41}$$

where $C_0 > 0$ depends only on I, I_1 and the Lipschitz constants of u and v. We now set

$$\delta = L^{-4}\left(\sup_{R^n\times[0,T]} |u-v|\right)^3 \tag{42}$$

and from (41), we obtain

$$\lambda \le C_0\left(L^{4/3} + L^{-4/3} + 1\right) \sup_{R^n\times[0,T]} |u-v|. \tag{43}$$

Let

$$\lambda = C_0\left(L^{4/3} + L^{-4/3} + 2\right) \sup |u-v|. \tag{44}$$

This leads to a contradiction with (43). Therefore, for the choice (44) of λ, $\omega(x,y,t)$ attains its maximum at $t = 0$, which is our claim. Hence,

$$\begin{aligned}u(x,t) - v(y,t) &- (4\delta)^{-1}|x-y|^4 - \lambda t \\ &\le \sup_{x,y\in R^n}\left(u(x,0) - v(y,0) - (4\delta)^{-1}|x-y|^4\right) \\ &\le \sup_{x,y\in R^n}\left(I(y) - I_1(y) + I(x) - I_1(x) - (4\delta)^{-1}|x-y|^4\right) \\ &\le \sup_{R^n}|I - I_1| + \sup_{|x-y|\ge 0}\left(I(x) - I(y) - (4\delta)^{-1}|x-y|^4\right) \\ &\le \sup_{R^n}|I - I_1| + \sup_{|x-y|\ge 0}\left(L|x-y| - (4\delta)^{-1}|x-y|^4\right).\end{aligned} \tag{45}$$

Noticing that $\sup_{r\geq 0}(Lr-(4\delta)^{-1}r^4)$ is achieved at $r=(\delta L)^{1/3}$, and letting $x=y$ in (45), from (42) and (44), we get

$$\begin{aligned}\sup_{R^n\times[0,T]}|u-v| &\leq \sup_{R^n}|I-I_1|+\frac{3}{4}\sup_{R^n\times[0,T]}|u-v|\\ &+C_0\left(L^{4/3}+L^{-4/3}+2\right)T\sup_{R^n\times[0,T]}|u-v|.\end{aligned}\tag{46}$$

Therefore, there exists $T_0>0$, sufficiently small ($T_0<1/8C_0(L^{4/3}+L^{-4/3}+2)$) such that from (46), we have

$$\sup_{R^n\times[0,T_0]}|u-v|\leq 8\sup_{R^n}|I-I_1|.\tag{47}$$

For large t, by iteration, we easily obtain

$$\sup_{R^n\times[0,T]}|u-v|\leq C(T)\sup_{R^n}|I-I_1|.$$

This proves the uniqueness and stability for u. ∎

4. NUMERICAL IMPLEMENTATION

The numerical implementation of the nonlinear diffusion equation (2) is based on the *upwind finite difference scheme* developed by Osher and Sethian [37] for curve evolution via level sets. Implementing the time derivative $\frac{\partial u}{\partial t}$ and the diffusive term $g(\nabla G_\sigma * I)|\nabla u|\,\mathrm{div}(\nabla u/|\nabla u|)$ presents no difficulties and is straightforward. $\frac{\partial u}{\partial t}$ is approximated by forward differences

$$\frac{u^{n+1}[i,j]-u^n[i,j]}{\triangle t},$$

and the diffusive term is approximated using the usual central differences, with

$$|\nabla u|\,\mathrm{div}\left(\frac{\nabla u}{|\nabla u|}\right)=\frac{u_y^2u_{xx}-2u_xu_yu_{xy}+u_x^2u_{yy}}{u_x^2+u_y^2}.$$

What does require special care is the implementation of the data term (in fact, an inflation term i.e., constant speed of expansion) $\beta|\nabla u|(u-I)/|u-I|$ and the "doublet" term $\nabla g\cdot\nabla u$ [16]. The inflation/ballooning term permits the development of first-order shocks, i.e., discontinuities in orientation of the boundary of a shape, where the derivative is not defined. Thus, we have to approximate the spatial derivative using the upwind finite difference scheme [37]. The "doublet" term permits the development of discontinuities which indicate the presence of object boundaries. In this case, we cannot use central finite differences but have to use forward or backward finite differences adaptively so that their directions are always away from the discontinuities. Let

$$\begin{aligned}D_i^+\phi^n[i,j]&=\phi^n[i+1,j]-\phi^n[i,j],\\ D_i^-\phi^n[i,j]&=\phi^n[i,j]-\phi^n[i-1,j],\\ D_j^+\phi^n[i,j]&=\phi^n[i,j+1]-\phi^n[i,j],\\ D_j^-\phi^n[i,j]&=\phi^n[i,j]-\phi^n[i,j-1],\\ D_i\phi^n[i,j]&=\frac{(\phi^n[i+1,j]-\phi^n[i-1,j])}{2},\\ D_j\phi^n[i,j]&=\frac{(\phi^n[i,j+1]-\phi^n[i,j-1])}{2},\end{aligned}$$

then

$$(\nabla g \cdot \nabla u)[i,j] = \max(D_i g^n[i,j],0) D_i^- u^n[i,j] + \min(D_i g^n[i,j],0) D_i^+ u^n[i,j] + \max(D_j g^n[i,j],0) D_j^- u^n[i,j] + \min(D_j g^n[i,j],0) D_j^+ u^n[i,j]$$

and

$$|\nabla u| = \left\{ \left(\max\left(D_i^- u^n[i,j],0\right)\right)^2 + \left(\min\left(D_i^+ u^n[i,j],0\right)\right)^2 + \left(\max\left(D_j^- u^n[i,j],0\right)\right)^2 + \left(\min\left(D_j^+ u^n[i,j],0\right)\right)^2 \right\}^{1/2}.$$

For a detailed discussion on this scheme, we refer the reader to [37,38].

As described earlier in Section 2, the nonlinear diffusion model can be embedded in a scale-space by using the parameter σ in the functional in equation (4). The scale-space tracking is posed as the steady state solution of the differential equation obtained by differentiating the equilibrium condition of the functional in equation (4) with respect to σ. Since this leads to a very complex differential equation which is impractical to implement, a simpler coupled system of equations was introduced in Section 2 by adopting the approach in [24]. For the sake of ease in reading, we repeat these coupled equations here:

$$\frac{\partial u}{\partial t} = -\nabla E_v(u,\sigma),$$
$$\frac{\partial \sigma}{\partial t} = -c_1 e^{-c_2 |\nabla E_v(u,\sigma)|},$$

with c_1 and c_2 being prespecified constants.

There are numerous techniques that exist in the numerical analysis literature for solving such first-order initial value problems. For example, one can use any of the following methods of solution listed in the order of sophistication: Euler's method, fourth-order Runge-Kutta method, or the Adams-Moulton predictor-corrector technique (see [39] for details on some of these methods). The Adams-Moulton and the Runge-Kutta methods have the advantage of being able to automatically determine an adaptive step size. Hence, they are more stable than the Euler scheme, but also more expensive (computationally). In our implementation, we used the explicit Euler method for reasons of computational cost.

The discrete version of these equations for the scale-space tracking is realized using an explicit Euler step in which time derivatives are approximated using forward difference formulas in time with a step size Δt. This gives us the following discrete equations:

$$\sigma^{t+1} = \sigma^t - (\Delta t) c_1 \exp -c_2 \left|\nabla E_v^t(u,\sigma)\right|, \tag{48}$$
$$u^{t+1} = u^t - (\Delta t) \nabla E_v^t\left(u^t, \sigma^t\right). \tag{49}$$

Note that the scale parameter σ is continuous in our formulation unlike in the multigrid formulation described in [26]. It is, however, worthwhile to investigate the application of the multigrid formulation described in Acton [26] to our model and will be the focus of our future effort in this context.

5. EXPERIMENTAL RESULTS

In this section, we present the application of our model for smoothing and segmentation of several image data sets. To test the effectiveness of this model, we first choose a synthetic image. Figure 2a shows the noiseless image which contains a triangle, a rectangle, a circle, and a thin ellipse. Figure 2b is obtained by adding Gaussian noise to (a), and the signal-to-noise ratio

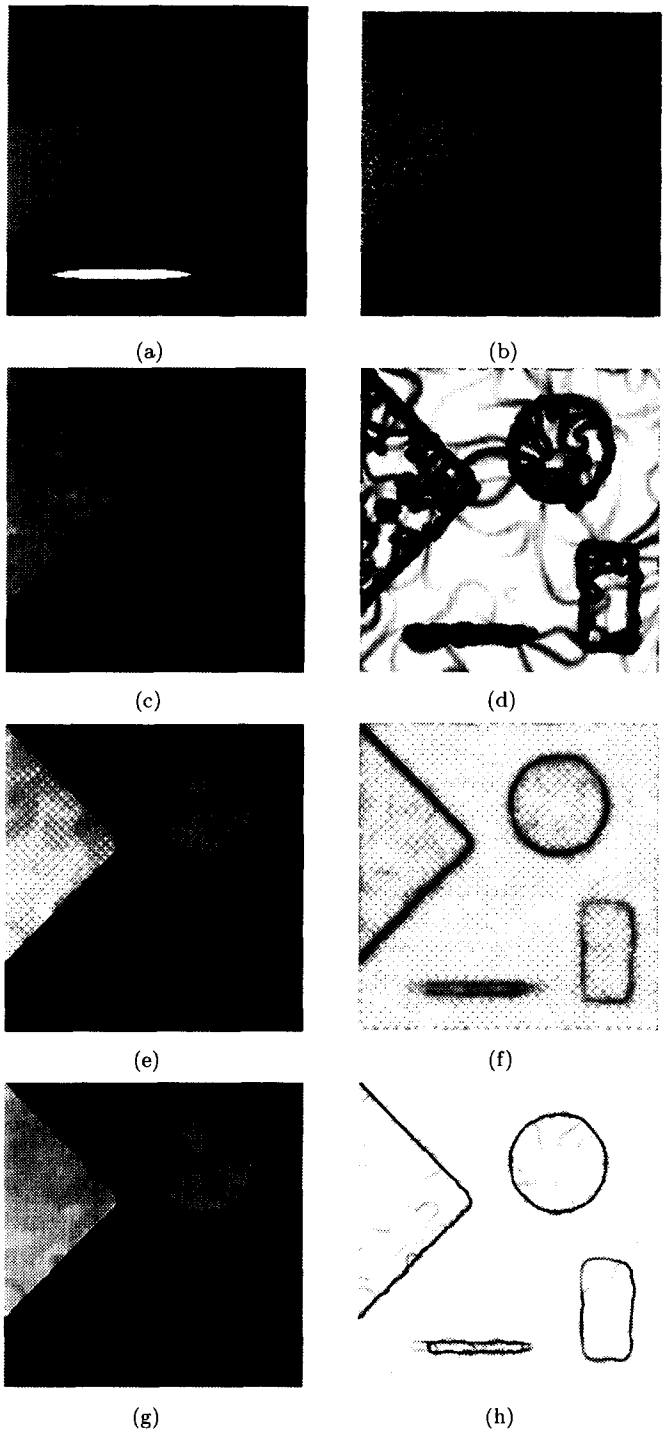

Figure 2. (a) Original image I, (b) I+Gaussian noise; smoothing and segmentation results from the competing and proposed methods, respectively. (c)–(d) The ALM model, (e)–(f) Shah's method, (g)–(h) our method.

(SNR: the ratio between the variance of the noise-free image and the variance of noise [1]) is 1 : 2. Figures 2c and 2d show the smoothing and segmentation results of the noisy synthetic image using the ALM model [7], where (c) is the smoothed image u and (d) shows the magnitude of $g(\nabla u)$. Figures 2e and 2f are smoothing and segmentation obtained using Shah's method [9], and finally Figures 2g and 2h are the smoothed image u and magnitude of $g(\nabla u)$ from our proposed method. The various parameter settings used to obtain these results were $\beta = 0.01$, $K = 200.0$ (note that $\sqrt{K}$ is the contrast parameter), number of iterations is 250, and the total

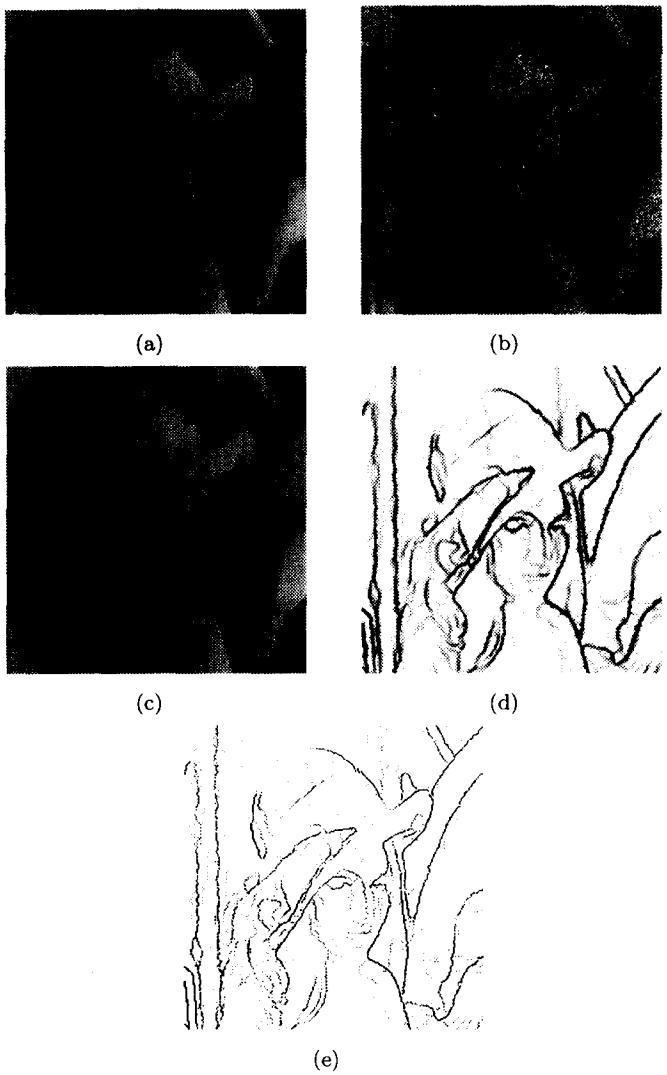

Figure 3. Smoothing and segmentation results of the noisy Lenna image (256 × 256) using single-PDE-based model; (a) original Lenna image; (b) Lenna image with Gaussian noise; (c) smoothed image u; (d) magnitude of $g(\nabla u)$; (e) edge map.

computing time on an Ultra Sparc-1 is 180 seconds. Note that our smoothing model has preserved the edges with minimal rounding of the sharp corners. In this and all the following examples, the stopping criterion for our nonlinear smoothing algorithm was a user specified tolerance (10^{-3}) on the norm of the difference between two consecutive iterates of u.

The second example is the smoothing and segmentation results of the popular Lenna image wherein we artificially added Gaussian noise (SNR = 3 : 1) to the image. The original Lenna image is shown in Figure 3a, Figure 3b is the noisy version of (a) obtained by adding Gaussian noise, Figure 3c depicts the smoothed image u, Figures 3d and 3e show the magnitude of $g(\nabla u)$ and the edge map, respectively. The edge map was obtained from the magnitude of $g(\nabla u)$ by performing a nonmaxima suppression. The parameter settings used to obtain these results were $\beta = 0.01$, $K = 200.0$, number of iterations is 120, and the total computing time on an Ultra Sparc-1 is 85 seconds. Once again, the results of smoothing and segmentation are of high quality and the latter may be used as a caricature of the original image leading to considerable image data compression.

Figure 4 presents the smoothing and segmentation of a CT chest scan. In this figure, (a) is the CT chest scan, (b) depicts the smoothed image u, (c) shows the magnitude of $g(\nabla u)$, and (d) is the edge map. The parameter settings used to obtain these results were $\beta = 0.005$, $K = 200.0$,

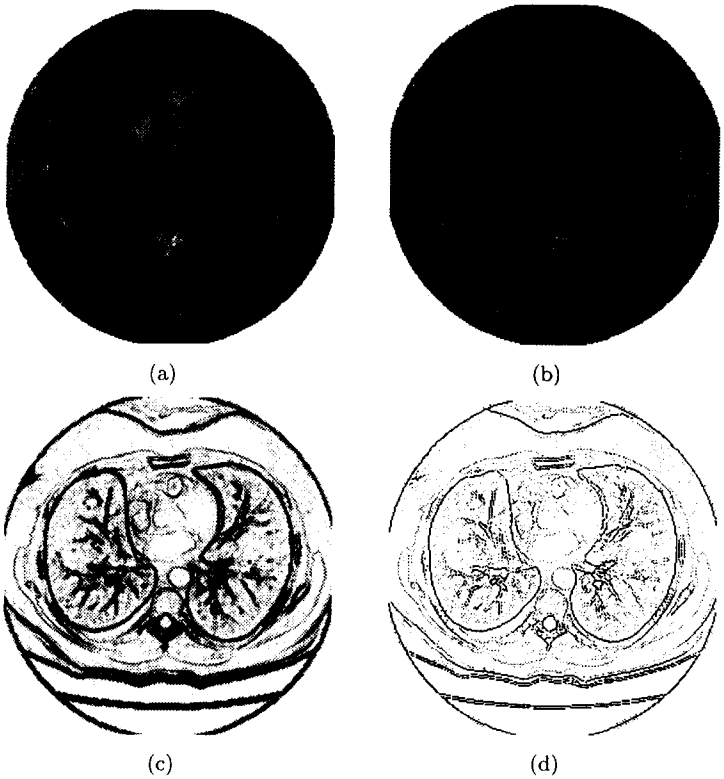

Figure 4. CT chest scan smoothing and segmentation. (a) Original image (512×512); (b) smoothed image u; (c) magnitude of $g(\nabla u)$; (d) edge map.

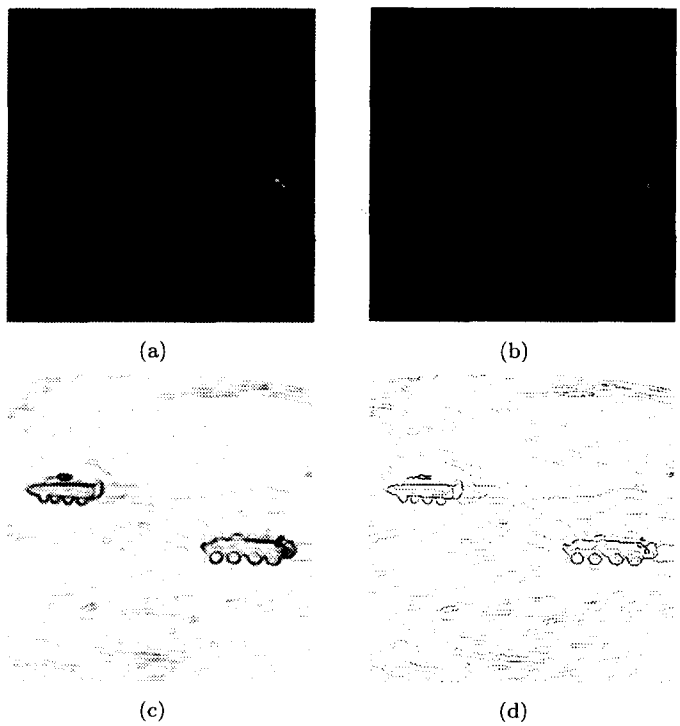

Figure 5. Smoothing and segmentation results of tanks image. (a) Original image (256 × 256); (b) smoothed image u; (c) magnitude of $g(\nabla u)$; (d) edge map. Parameters: $\beta = 0.05$, $K = 200.0$, number of iterations is 20, and the total computing time on an Ultra Sparc-1 is 7 seconds.

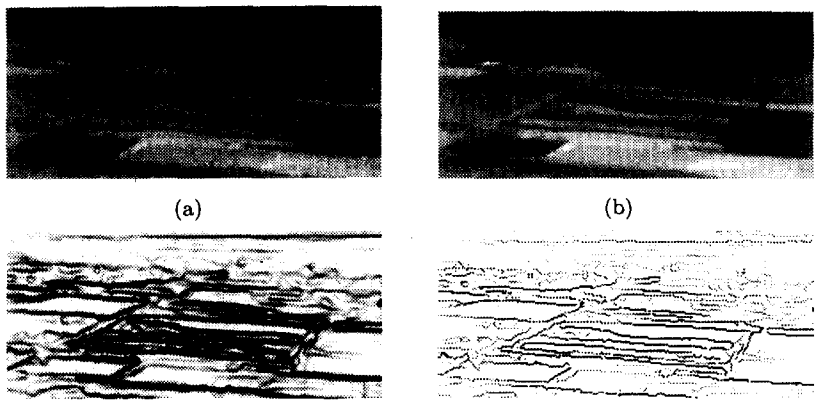

(a) (b)

(c) (d)

Figure 6. Smoothing and segmentation results of one of the TI Infra-Red High-Value Target Acquisition (IRHVTA) Data. (a) Original image (256 × 256); (b) smoothed image u; (c) magnitude of $g(\nabla u)$; (d) edge map. Parameters: $\beta = 0.05$, $K = 100.0$, number of iterations is 20, and the total computing time on an Ultra Sparc-1 is 7 seconds.

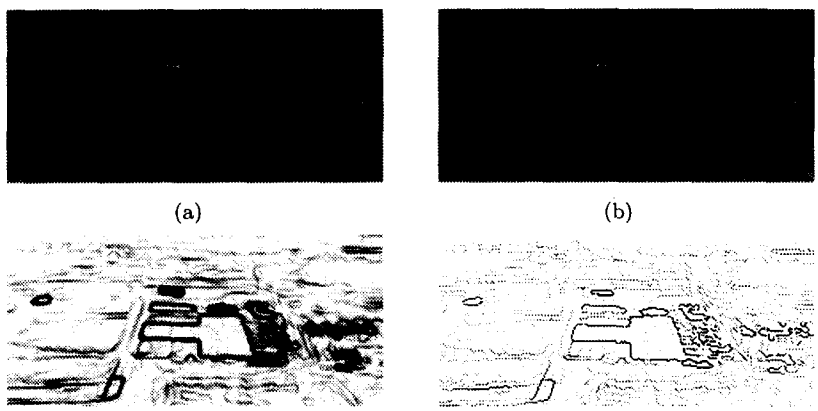

(a) (b)

(c) (d)

Figure 7. Smoothing and segmentation results of one of TI Infra-Red High-Value Target Acquisition (IRHVTA) Data. (a) Original image (256 × 256); (b) smoothed image u; (c) magnitude of $g(\nabla u)$; (d) edge map. Parameters: $\beta = 0.05$, $K = 200.0$, number of iterations is 10, and the total computing time on an Ultra Sparc-1 is 4 seconds.

number of iterations is 10, and the total compute time on an Ultra Sparc-1 is 15 seconds. We can see that some of the "important" details which are unclear in the original image are enhanced in the smoothing and segmentation results.

Each of the following examples in Figures 5–7 presents four images: (a) is the original image, (b) shows the smoothing result, and (c) and (d) are the segmentation results from our nonlinear diffusion model. These images are infrared images for automatic target tracking applications and some of them are the Texas Instruments (TI) high value target acquisition images.

6. CONCLUSION

We have proposed a unified PDE-based image denoising and segmentation algorithm based on nonlinear diffusion augmented by reactive terms. Our model is a unification of the popular ALM model [7] and the model due to Caselles *et al.* [16]. We experimentally show that the unified model outperforms the ALM model as well as the more recent model by Shah [9].

We prove the existence, uniqueness, and stability of the viscosity solution of our model. For a fast implementation, we embed this model in a scale space and achieve scale space tracking via a dynamical system of coupled differential equations. The scale space tracking is implemented

using a multigrid scheme. We present experiments depicting the performance of our model on several image data sets. Our future efforts will be focused on a 3-D implementation of our model and testing on volume images, e.g., magnetic resonance (MR) and CT images.

REFERENCES

1. J.S. Lim, *Two-Dimensional Signal and Image Processing*, Prentice Hall, Englewood Cliffs, NJ, (1990).
2. S. Geman and D. Geman, Stochastic relaxation, Gibbs distributions and Bayesian restoration of images, *IEEE Trans. on Pattern Analysis and Machine Intelligence* **6**, 721–741, (1984).
3. D. Geiger and A. Yuille, A common framework for image segmentation, *International Journal of Computer Vision* **6**, 227–243, (1991).
4. P. Perona and J. Malik, Scale-space and edge detection using anisotropic diffusion, *IEEE Trans. PAMI* **12**, (7), 629–639, (1990).
5. F. Catte, P.L. Lions, J.M. Morel and T. Coll, Image selective smoothing and edge detection by nonlinear diffusion, *SIAM Journal of Numerical Analysis* **29**, 182–193, (1992).
6. M. Nitzberg and T. Shiota, Nonlinear image filtering with edge and corner enhancement, *IEEE Transactions on Pattern Analysis and Machine Intelligence* **14** (8), 826–832, (1992).
7. L. Alvarez, P.L. Lions and J.M. Morel, Image selective smoothing and edge detection by nonlinear diffusion. II, *SIAM J. Numer. Anal.* **29** (3), 845–866, (June 1992).
8. P.J. Olver, G. Sapiro and A. Tannenbaum, Invariant geometric evolutions of surfaces and volumetric smoothing, *SIAM J. Appl. Math.* **57**, 176–194, (1997).
9. J. Shah, A common framework for curve evolution, segmentation and anisotropic diffusion, In *IEEE Conf. on Computer Vision and Pattern Recognition*, (1996).
10. J. Weickert, A review of nonlinear diffusion filtering, In *Scale-Space Theory in Computer Vision*, (Edited by B. ter Haar Romney, L. Florack, J. Koenderink and M. Viergever), *Lecture Notes in Computer Science*, Vol. 1252, pp. 3–28, Springer-Verlag, (1997).
11. B.B. Kimia, A.R. Tannenbaum and S.W. Zucker, Shapes, shocks, and deformations I: The components of shape and the reaction-diffusion space, *Intl. Journal of Computer Vision* **15**, 189–224, (1995).
12. H. Tek and B.B. Kimia, Image segmentation by reaction-diffusion bubbles, In *Fifth International Conference on Computer Vision*, (1995).
13. R. Malladi, J.A. Sethian and B.C. Vemuri, Evolutionary fronts for topology independent shape modeling and recovering, In *Proc. ECCV*, (1995).
14. R. Malladi, J.A. Sethian and B.C. Vemuri, Shape modeling with front propagation: A level set approach, *IEEE Trans. PAMI* **17**, (2), 158–175, (1995).
15. V. Caselles, F. Catte, T. Coll and F. Dibos, A geometric method for active contours, *Numerische Mathematik* **66**, (1993).
16. V. Caselles, R. Kimmel and G. Sapiro, Geodesic active contours, In *Fifth International Conference on Computer Vision*, (1995).
17. S. Kichenassamy, A. Kumar, P. Olver, A. Tannenbaum and A. Yezzi, Gradient flows and geometric active contour models, In *Fifth International Conference on Computer Vision*, (1995).
18. M. Kass, A. Witkin and D. Terzopoulos, Snakes: Active contour models, *Int. Journal of Computer Vision* **1** (4), 321–332, (1988).
19. D. Terzopoulos, A. Witkin and M. Kass, Constraints on deformable models: Recovering 3D shape and nonrigid motion, *Artificial Intelligence* **36**, 91–123, (1988).
20. T. Mclnerney and D. Terzopoulos, Deformable models in medical image analysis: A survey, *Medical Image Analysis* **1** (2), (1996).
21. E.J. Pauwels, P. Fiddelaers and L.J. Van Gool, Shape-extraction for curves using geometry-driven diffusion and functional optimization, In *Proc. of IEEE Intl. Conf. on Compu. Vision (ICCV)*, pp. 396–401, (1995).
22. R. Malladi and J.A. Sethian, A unified approach to noise removal, image enhancement and shape recovery, *IEEE Trans. on Image Processing* **5** (11), 1554–1568, (1996).
23. R. Kimmel, N. Sochen and R. Malladi, Images as embedding maps and minimal surfaces: Movies, color and volumetric medical images, In *Proc. of the IEEE Conf. on Computer Vision and Pattern Recognition*, pp. 350–355, (June 1997).
24. A. Witkin, D. Terzopoulos and M. Kass, Signal matching through scale space, *Int. J. Comput. Vision* **1**, 133–144, (1987).
25. G. Whitten, Scale space tracking and deformable sheet models for computational vision, *IEEE Trans. Patt. Anal. Machine Intell.* **15** (7), 697–706, (July 1993).
26. S. Acton, Multigrid anisotropic diffusion, *IEEE Transactions on Image Processing* **7** (3), 280–291, (1998).
27. V. Caselles, R. Kimmel and G. Sapiro, Geodesic active contours, *Intl. Journal of Computer Vision* **22**, 61–97, (1997).
28. G. Sapiro, Vector-valued active contours, In *IEEE Proc. of the CVPR*, pp. 680–685, IEEE Computer Soc. Press, (1996).
29. G. Sapiro and D.L. Ringach, Anisotropic diffusion of multivalued images with applications to color filtering, *IEEE Trans. on Image Processing* **5**, 1582–1586, (1996).

30. P. Charbonnier, L. Blanc-Feraud, G. Aubert and M. Barlaud, Two deterministic half-quadratic regularization algorithms for computed imaging, In *Proc. of the IEEE Intl. Conf. on Image Processing (ICIP)*, Vol. 2, pp. 168–172, IEEE Computer Society Press, (1994).
31. L. Alvarez and J. Esclarín, Image quantization using reaction-diffusion equations, *SIAM J. Appl. Math.* **57** (1), 153-175, (1997).
32. M.G. Crandall, H. Ishii and P.L. Lions, User's guide to viscosity solution of second order partial differential equation, *Bulletin of the American Mathematical Society* **27** (1), 1–67, (1992).
33. L.C. Evans and J. Spruck, Motion of level sets by mean curvature. I, *J. Differential Geometry* **33**, 635–681, (1991).
34. Y.-G. Chen, Y. Giga and S. Goto, Uniqueness and existence of viscosity solutions of generalized mean curvature flow equations, *Journal of Differential Geometry* **33**, 749–786, (1991).
35. O.A. Ladyzhenskaya, V.A. Solonnikov and N.N. Uraltseva, *Linear and Quasilinear Equations of Parabolic Type*, American Mathematical Society, Providence, RI, (1968).
36. H. Brezis, *Analyse Fonctionnelle, Théorie et Applicatons*, Masson, Paris, (1987).
37. S.J. Osher and J.A. Sethian, Fronts propagation with curvature dependent speed: Algorithms based on Hamilton-Jacobi formulations, *Journal of Computational Physics* **79**, 12–49, (1988).
38. R. Malladi, J. Sethian and B.C. Vemuri, A fast level set based algorithm for topology-independent shape modeling, *J. Mathematical Imaging and Vision* **6**, 269–289, (1996).
39. G. Dahlquist and A. Björck, *Numerical Methods*, Prentice-Hall, (1974).